Aswan University Journal of Sciences and Technology Volume 5, issue 3, September 2025

Investigating the behaviour of High-Strength Self-Compacted Reinforced Concrete Slender Beams experimentally and numerically

Mohamed. O. Elsibaey [1*], Mona Saleh [2], Zakaria. H. Awadallah [3], Abdo Khalaf [3], Ayman Othman[1], Mohamed Zakaria[1]

[1]Civil Engineering Department, Aswan University, Aswan, Egypt; Mohamedelsibaey2014@gmail.com, Ay_Othman@mail.com, M.zakaria2009@gmail.com

[2]Civil Engineering Department, High Institute for Engineering and Technology, Sohag, Egypt; Monaesmail093@gmail.com

[3]Civil Engineering Department, Alazhr University, Qena, Egypt; Zakariahameed44@yahoo.com, Abdounagah@gmail.com

Abstract

High-strength self-compacted reinforced concrete (HS-SCRC) slender beams are gaining popularity in modern construction due to their efficiency and reduced material usage. To comprehend the flexural behaviour, failure processes, and serviceability performance of HS-SCRC thin beams, this work combines experimental and computational analyses. These beams, characterized by high slenderness and compressive strength, exhibit complex behaviour under static loading. This study investigates their flexural behaviour, failure modes, and serviceability through experimental and numerical approaches. Ten beam specimens with varying compressive strengths (25, 30, 40 and 55 MPa), reinforcement ratios (4ø12, 6 ø12 and 4ø10) and shear span-to-depth ratios (1.75, 2 and 2.22) were tested under four-point bending. Finite element models were developed in ABAQUS using the Concrete Damaged Plasticity (CDP) model and embedded reinforcement to simulate the performance of beams. Numerical results closely matched the experiments, with average deviations of 6.86% in cracking load, 3.48% in ultimate load, and 8.82% in deflection. The validated models enabled extended parametric analysis, confirming their effectiveness in capturing nonlinear behaviour. The findings enhance understanding of HS-SCRC slender beams and support future developments in structural design and code provisions.

Keywords: Slender RC beams; Finite element modelling; Cracking behavior; Abaqus; Static flexural loading.

1. Introduction

Slender reinforced concrete (RC) elements are widely used in modern infrastructure, particularly in high-rise buildings, long-span bridges, and industrial facilities, where reducing member self-weight and increasing span efficiency are paramount. These elements, characterized by a high span-to-depth ratio, are structurally efficient but often susceptible to complex failure mechanisms, including lateral instability, premature cracking, and excessive deflection. Unlike conventional RC beams, slender beams demand careful evaluation of their structural response under service and ultimate limit states due to their geometric proportions and sensitivity to second-order effects. Despite extensive research spanning over seven decades, the complete understanding of slender beam behaviour under flexural loading remains elusive.

*Corresponding author E-mail: mohamedelsibaey2014@gmail.com
Received July 22, 2025, received in revised form, August 01, 2025, accepted August 10, 2025.

(ASWJST 2021/ printed ISSN: 2735-3087 and on-line ISSN: 2735-3095) https://journals.aswu.edu.eg/stjournal

Numerous empirical and semi-empirical models have been proposed to estimate the behaviour of RC beams; however, these models typically lack a strong theoretical foundation and are usually applicable only within limited ranges of material characteristics and structural geometries. Most of these models are derived from experimental curve fitting and are unable to capture the full spectrum of nonlinearity associated with slender members, especially when high-performance concrete or innovative reinforcement layouts are involved.

The behaviour of slender beams has become even more complex in recent years due to the introduction of self-compacted concrete (SCC) and high-strength concrete (HSC). HSC offers superior compressive strength and reduced section sizes, while SCC enhances workability and compaction quality, particularly in densely reinforced members. The combination of these materials - high-strength self-compacted reinforced concrete (HS-SCRC) - has proven to be structurally advantageous but presents new challenges in predicting cracking behaviour, ductility, and failure mechanisms, especially when used in slender members. To overcome these challenges, finite element analysis (FEA) has emerged as a valuable tool for simulating the nonlinear behaviour of RC structures. Modern FEA platforms such as ABAQUS/CAE facilitate the accurate modelling of material heterogeneity, cracking propagation, strain localization, and interaction between concrete and steel reinforcement. These tools allow for the virtual prototyping of structural components under diverse loading and boundary conditions, reducing the dependency on costly and time-consuming experimental campaigns. When calibrated properly, numerical models can provide insight into internal stress states, deformation patterns, and the impact of key design variables that are difficult to observe directly in physical experiments.

Several recent studies have attempted to model the behaviour of RC beams using advanced numerical tools. For instance, **Omar Jum'ah et al. [1]** investigated the shear performance of fiber-reinforced self-compacting concrete beams with varying concrete grades (28 MPa, 60 MPa, and 100 MPa) and fiber contents. Their results highlighted the importance of both concrete strength and fiber volume in influencing the shear capacity of deep and slender beams. **Thamer Hussein et al. [2]** examined RC deep flanged beams with recycled concrete aggregates (RCA) and concluded that increasing RCA content significantly affects cracking and strength. Their study also confirmed that higher *a/d* ratios correlate with reduced ultimate loads, aligning with arch action theory. **Kalkan et al. [3,4]** studied the torsional behaviour and lateral-torsional buckling of slender RC beams. They showed that high-strength concrete prolongs the elastic behaviour before instability and that torsional cracks tend to initiate near support regions under varying moment conditions. Similarly, **Tahenni et al. [5]** used nonlinear finite element modelling (NLFEA) via **ANSYS [6]** to study the influence of diagonal cracking in beams with and without transverse reinforcement. Their results emphasised that HSC beams without stirrups exhibit brittle shear failure, while the inclusion of transverse reinforcement shifts failure toward a more ductile flexural mode. Despite these advances, a clear knowledge gap persists regarding the combined use of HS-SCRC in slender beams and the corresponding validation of numerical models through experimental testing.

The present study addresses this gap by conducting a comprehensive investigation that combines experimental data and finite element simulations to examine the influence of concrete strength, reinforcement ratio, and shear span-to-depth ratio on the flexural behaviour of HS-SCRC slender beams. By using this comprehensive approach, the study seeks to enhance prediction accuracy and

support the development of dependable design methods for slender high-performance concrete structures.

2. Theoretical Investigations

2.1. General Overview

A total of ten high-strength self-compacting reinforced concrete (HS-SCRC) beams were subjected to numerical analysis under static loading conditions using **ABAQUS** software **[7]**. The specimens were categorised into two groups. The first group included a single non-slender beam, designed as a control specimen, with dimensions of 120 mm in width, 750 mm in depth, and 2000 mm in length. The second group comprised nine slender beams, each measuring 100 mm in width, 750 mm in depth, and 4000 mm in length. The geometrical and reinforcement details of all beam specimens are presented in **Table 1.**

Table 1: Test beam data.

Beam Label	B×D×L *(mm)*	*a/d*	f_c^- ($_{MPa}$)	Main Reinforcement	Secondary Reinforcement	Type
Beam 1	120×750×2000	1	25	4 Ø16	4 Ø16	Non-Slender (Shear)
Beam 2	100×750×4000	2.22	30	4 Ø16	4 Ø16	Slender (flexural)
Beam 3	100×750×4000	2	55	4 Ø12	4 Ø12	Slender (flexural)
Beam 4	100×750×4000	2	55	6 Ø12	6 Ø12	Slender (flexural)
Beam 5	100×750×4000	2.22	45	4 Ø16	4 Ø16	Slender (flexural)
Beam 6	100×750×4000	2.22	55	4 Ø16	4 Ø16	Slender (flexural)
Beam 7	100×750×4000	2	55	4 Ø10	4 Ø10	Slender (flexural)
Beam 8	100×750×4000	1.75	55	6 Ø12	4 Ø12	Slender (flexural)
Beam 9	100×750×4000	2	55	6 Ø12	4 Ø12	Slender (flexural)
Beam 10	100×750×4000	2.22	55	6 Ø12	4 Ø12	Slender (flexural)

- Beams 2,5 and 6 are varied in the concrete strength.
- Beams 3,4 and 7 are varied in the main reinforcement ratio.
- Beams 8,9 and 10 are varied in *a/d*.
- Long.Reinf$_{comp}$ Longitudinal compression steel reinforcement.
- Long.Reinf$_{ten}$ Longitudinal tension steel reinforcement.

2.2. Finite Element Modelling

The finite element model was developed using two primary types of elements: solid elements and truss (wire) elements. Within the ABAQUS model tree, the Part module was employed to define the geometry and assign the appropriate element types required for constructing the complete finite element representation of the beams.

2.3. Material properties

2.3.1. Solid Element

Slender concrete beams were modelled using the eight-node linear brick element with reduced integration, **C3D8R**, as recommended by **Elwakkad et al**. **[8]**. Each node of this element possesses three translational degrees of freedom, allowing it to accurately simulate deformation behaviour under applied loads **[9]**. The C3D8R element was selected due to its capability to define concrete boundaries and facilitate the specification of contact surfaces necessary for load application and interaction modelling. Moreover, it is well-suited for nonlinear static and dynamic analyses, as well as large displacement problems involving finite strain and rotation. In this study, the same element type was also used to model the steel loading plates and roller support assemblies.

2.3.2. Truss Element

Truss (wire) elements are one-dimensional members capable of transmitting axial forces - either tensile or compressive - while offering no resistance to bending or shear. Due to this characteristic, they are particularly suitable for modelling reinforcement bars embedded within concrete elements, as recommended by **Kenea and Megersa [10]** and **Attia et al. [11]**. In this study, the T3D2 element type was adopted to represent both the longitudinal steel reinforcement and stirrups. These elements were defined as embedded reinforcements within the concrete matrix, ensuring full bond compatibility between steel and concrete through the embedded region technique.

2.4. Material Modelling

While the material properties of the finite elements were defined in the modelling process, obtaining accurate and high-quality data, especially for complex behaviours such as material damage, remains a significant challenge. The reliability and precision of finite element analysis outcomes are heavily influenced by the accuracy and completeness of the input data. In this study, two distinct material models available in ABAQUS were employed to simulate the mechanical behaviour of the concrete beams: The Concrete Damaged Plasticity (CDP) model for the concrete, and an elastic–plastic model for the reinforcing steel. These models were selected to capture both the nonlinear inelastic behaviour and the damage evolution observed in the tested slender beam specimens.

2.4.1. Concrete Damaged Plasticity Model (CDP)

The concrete material was represented using a continuum damage plasticity (CDP) model grounded in plasticity theory. As demonstrated in **Fig. 1**, this model effectively simulates the nonlinear response of concrete under both uniaxial tension and compression. It captures the development of micro-cracks that occur once the concrete reaches its failure stress in tension or compression. Beyond this failure point, the stress–strain behaviour follows a softening trend, reflecting the gradual loss of stiffness and strength.

In uniaxial compression, the initial stress–strain relationship is linear until the material reaches its yield point, defined by its compressive strength. After yielding, the response includes plastic hardening followed by strain softening in the post-peak phase, as shown in **Fig. 1(b).** Under tensile loading, the response progresses through a tension stiffening stage before entering the softening region, illustrated in **Fig. 1(a).**

The unloading behaviour from any point along the inelastic strain path is defined by the degradation parameters of the material and can be described mathematically as **[12]**:

$$f_t = E_c\,(\varepsilon_t - \varepsilon_t^{\,pl})\,(1 - d_t) \qquad \textbf{(1)}$$

$$f_c = E_c\,(\varepsilon_c - \varepsilon_c^{\,pl})\,(1 - d_c) \qquad \textbf{(2)}$$

Where:

ft and fc are the tensile and compressive stresses, respectively.
Ec is the modulus of elasticity of concrete.
εt and εc are the total tensile and compressive strains.
$\varepsilon t\ pl$ and $\varepsilon c\ pl$ are the corresponding plastic strains.
dt , dc are the damage parameters in tension and compression, respectively.

Then, the effective tensile and compressive cohesion stresses of concrete are estimated as:

$$\bar{f}_c = \frac{f_c}{(1-d_c)} = E_c(\varepsilon_c - \varepsilon_c^{pl}) \quad \textbf{(3)}$$

$$\bar{f}_t = \frac{f_t}{(1-d_t)} = E_c(\varepsilon_t - \varepsilon_t^{pl}) \quad \textbf{(4)}$$

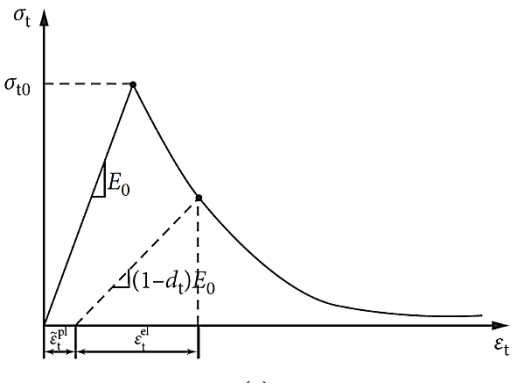

(a) Tensile behavior associated with tension stiffening.

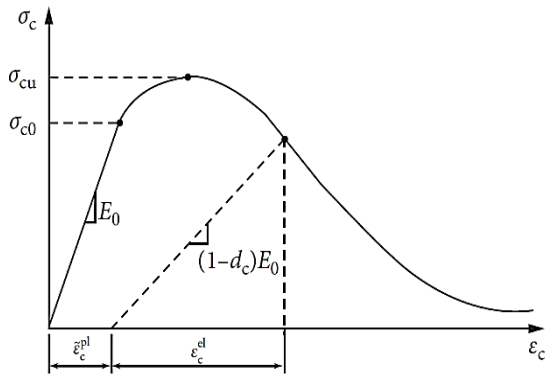

(b) Compressive behavior associated with compression hardening.

Figure 1: Concrete damaged plasticity model **[13].**

The post-failure behaviour of reinforced concrete is represented through the post-failure stress as a function of cracking strain ε_t^{ck} and $\varepsilon_c^{ck,}$ which are defined as the total strain minus the elastic strain corresponding to the undamaged material, and tension stiffening data are given in terms of the cracking strains **[13].** When unloading data is available, programming automatically converts the cracking strain values to plastic strain values using the following relationships:

$$\varepsilon_t^{pl} = \varepsilon_t^{ck} - \frac{d_t}{(1-d_t)} \times \frac{f_t}{E_c} \quad \textbf{(5)}$$

$$\varepsilon_c^{pl} = \varepsilon_c^{ck} - \frac{d_c}{(1-d_c)} \times \frac{f_c}{E_c} \quad \textbf{(6)}$$

Tables 2 and 3 list elastic properties and concrete damaged plasticity model parameters used to represent concrete. The modulus of elasticity of concrete was calculated **[14]** using the following formula:

$$E_c = 4400\sqrt{f_{cu}} \quad \text{N/mm}^2 \quad \textbf{(7)}$$

Where (f_{cu}) is the compressive strength of the standard cubes at 28 days.

Table 2: Elastic properties of concrete **[13]**.

Parameter	CDP/25 MPa	CDP/30 MPa	CDP/45 MPa	CDP/55 MPa
Density, kg/m^3	2400	2400	2400	2400
Modulus of elasticity (E)	22000	24099.8	29516.1	33509.4
Poisson's ratio (υ)	0.2	0.2	0.21	0.21

2.4.2. Elastic-Plastic Model

When the Young's modulus, or elastic modulus, introduced by the steel stiffness, remains constant at low strain magnitudes, the steel of the reinforcing bars exhibits roughly linear elastic behaviour. At increased strain levels, it demonstrates inelastic and nonlinear behaviour typical of plastic deformation.

Steel's yield point and post-yield hardening serve to define its plastic behaviour. The yield point on a material's stress-strain curve marks the transition from elastic to plastic behaviour. Only elastic strains, which recover if the applied force is withdrawn, are produced when the steel is deformed before it reaches the yield point. However, as soon as the steel's tension reaches its yield stress, permanent (plastic) deformation starts to happen. As the metal deforms in the post-yielding zone, elastic and plastic strains progressively increase. As soon as the steel yields, its stiffness reduces. The steel material's plastic deformation raises its yield stress for incoming loads. The elastic-plastic material model in ABAQUS was used to represent the behaviour of steel bars. The simplified stress-strain curve using the experimental values was considered in estimating the steel's plastic behaviour. **Figure 2** illustrates the stress-strain curve of a bilinear elastic-plastic material.

Table 3: Concrete damaged plasticity parameters **[13]**.

Parameter	CDP/25 MPa	CDP/30 MPa	CDP/45 MPa	CDP/55 MPa
Dilation angle (degree)	36	36	41	43
Eccentricity	0.12	0.12	0.12	0.122
fb0/fc0	1.36	1.36	1.35	1.36
K	0.67	0.67	0.67	0.67
Viscosity parameter	0.00001	0.00001	0.00001	0.00001
Compressive ultimate stress, MPa	29.13	31.03	46.59	57.9
Tensile ultimate stress, MPa	2.5	3	4.49	5.5

Elastic modulus E_s, yield stress f_y, ultimate stress f_u, and Poisson's ratio were extracted from the experimental data to determine the metallic reinforcement's elastic-plastic behaviour. **Table 4** lists mechanical properties values used in finite element modelling to define material models of metallic reinforcement.

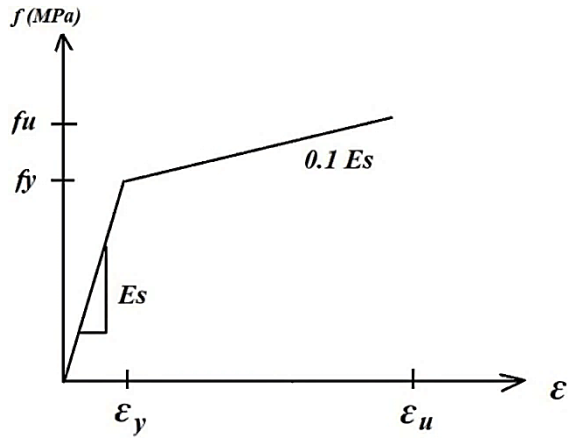

Figure 2: Bilinear elastic-plastic behaviour [**15**].

Table 4: The Mechanical properties of metallic reinforcement.

Parameter	High Tensile Steel	Mild Steel
Density, kg/m^3	7860	7860
Modulus of elasticity (Es), MPa	210000	200000
Poisson's ratio (υ)	0.3	0.3
Yield stress, MPa	360	240
Ultimate strength, MPa	520	355

3. RESULTS AND DISCUSSIONS

3.1. General Behaviour and Failure Modes

The numerical simulations performed using ABAQUS/CAE effectively replicated the overall structural performance of high-strength self-compacting reinforced concrete (HS-SCRC) slender beams under static loading, closely aligning with the experimental findings. In all specimens except beam **B1**, flexural failure was the predominant mode. Vertical flexural cracks originated in the tensile zone at mid-span and extended upward as the load increased. The ABAQUS model captured this behaviour through rising tensile damage values exceeding 0.9 in the mid-span area, which corresponded well with the physical crack patterns observed during testing.

In the experimental results, the beam **B1** experienced a shear-dominated failure, marked by the formation of diagonal cracks near the support regions. This failure mode was also accurately reflected in the finite element model, where high tension damage values were concentrated around the supports, indicating shear stress as the primary cause. In contrast, the remaining slender beams demonstrated ductile flexural behaviour, showing a gradual decline in load-bearing capacity after reaching the peak load. **Figure 3** illustrates the FE model for beam **B1**, showing the distribution of stresses and deformations under loading. As the load gradually increased, microcracks began to appear, represented by a light red colour with damage values between 0 and 0.5. With further loading, these microcracks progressively developed into deeper cracks. The first visible crack in the FE model occurred at a load of 12.8 tons, with the damage colour intensifying to dark red, eventually leading to complete failure at 63 tons. The failure mode identified for this beam was shear failure.

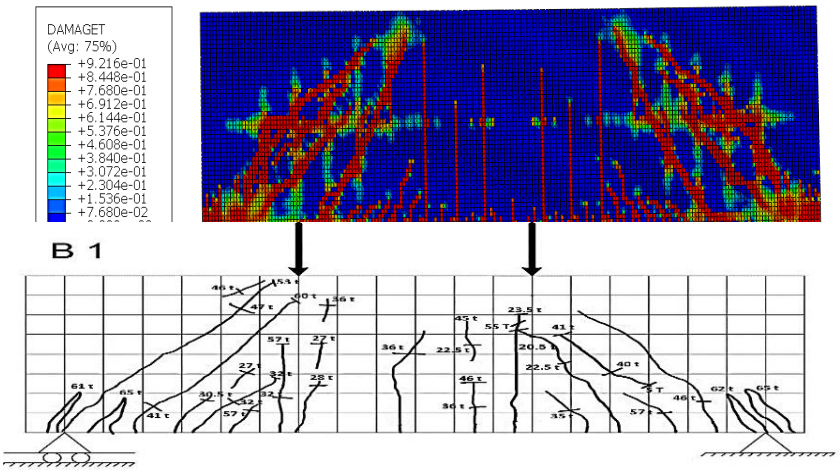

Figure 3: Pattern of cracks and method of failure for beam (**B1**).

- **Effect of Concrete Compressive Strength**

The compressive strength of concrete had a pronounced impact on the beam performance. Numerically, as the concrete strength increased from 30 MPa (**B2**) to 55 MPa (**B6**), both the stiffness and ultimate load capacity improved. For instance, the simulated ultimate load for **B2** was 166.93 kN, while **B6** reached 216.31 kN. Corresponding mid-span deflections also decreased from 10.66 mm in **B2** to 10.34 mm in **B6**. The CDP model successfully captured the delayed cracking and reduced strain concentrations in higher-strength concrete. The tension damage values developed more slowly in high-strength beams, reflecting the material's greater resistance to tensile failure, as shown in **Fig. 4.**

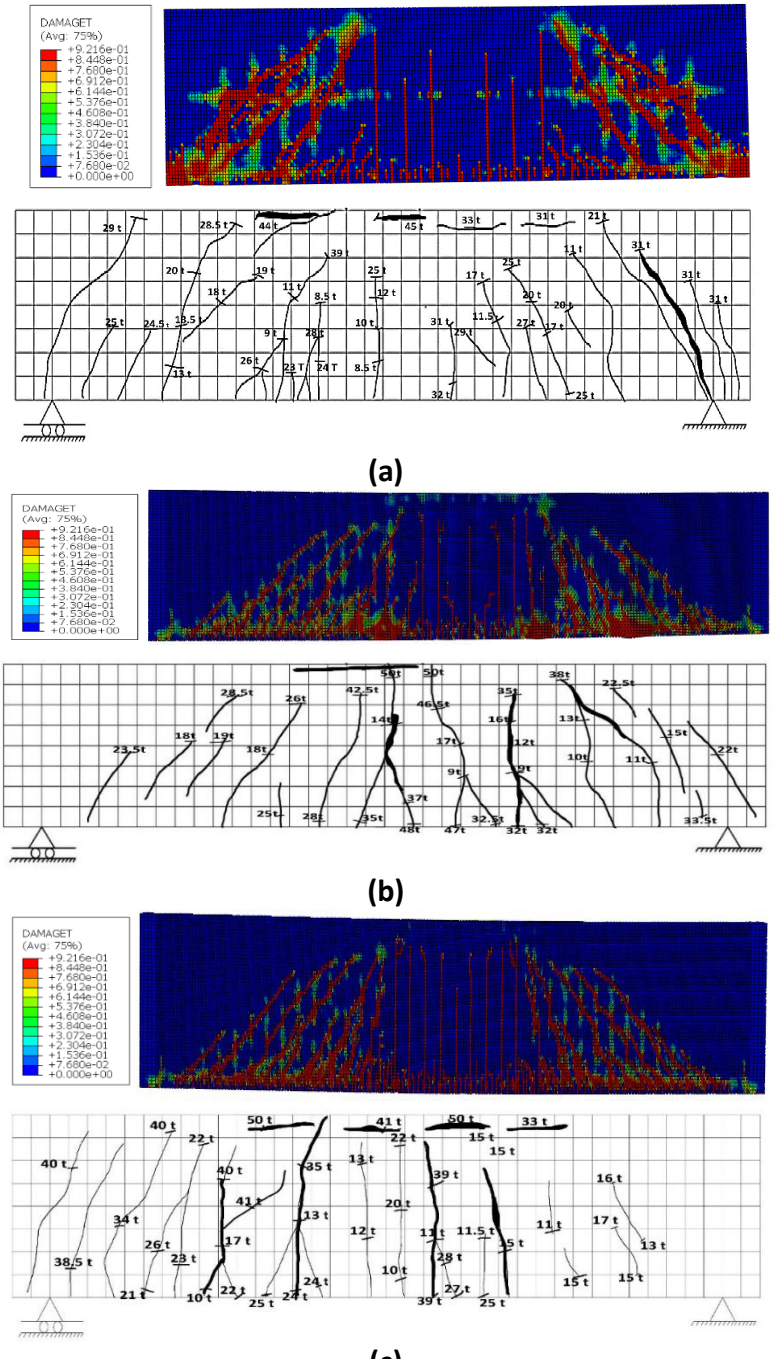

Figure 4: Effect of Concrete Strength on the crack patterns. Specimen **B2,** (b) Specimen **B5,** (c) Specimen **B6.**

In the experimental results, similar trends were observed. Beams with higher concrete strength developed fewer and narrower cracks. The crack propagation was more localised, and the failure mode appeared more brittle, particularly in **B6**. The increased concrete strength enhanced the modulus of elasticity, resulting in stiffer behaviour and better energy dissipation under load. These observations align well with the numerical model outputs, indicating strong agreement between the practical and theoretical assessments. The model was especially effective in capturing the change in failure mechanism and stiffness associated with varying compressive strength.

- **Effect of Longitudinal Reinforcement Ratio**

The variation in longitudinal reinforcement ratio significantly influenced the structural response in both experimental and numerical studies. In the FE simulations, an increase in reinforcement ratio led to higher load capacity, improved ductility, and lower steel strain levels. Beam B4, which had the highest reinforcement ratio, achieved an ultimate load of 191.29 kN and exhibited stable post-yield behaviour. In contrast, **B7**, with the lowest reinforcement, failed at 154.87 kN and showed early yielding of the reinforcement and excessive deflection. The tension damage in the ABAQUS model for **B7** was more widespread, consistent with the observed experimental cracking.

Experimentally, **B4** also demonstrated superior performance, with narrower cracks, smaller deflections, and delayed yielding of steel bars. The measured deflection at peak load was significantly lower in **B4** compared to **B7**. The use of additional reinforcement improved stress distribution, reduced curvature, and controlled crack spacing, leading to a more desirable failure mode. These practical findings reinforce the accuracy of the numerical modelling and highlight the importance of reinforcement ratio in slender beam design. The FE model's ability to replicate both the magnitude and pattern of structural response validates its application in future parametric studies. **Figure 5** illustrates the effect of reinforcement ratio on the crack patterns.

- **Effect of Shear Span-to-Depth Ratio (a/d)**

The influence of the shear span-to-depth ratio (*a/d*) was evident in both sets of results. Beams with lower *a/d* ratios, such as **B8** (*a/d* = 1.75), benefited from enhanced arch action and exhibited mixed flexure-shear behaviour. The numerical ultimate load for **B8** was 200.37 kN, and the crack distribution was denser near the supports. As *a/d* increased to 2.22 in **B10**, the behaviour transitioned to pure flexural failure, with vertical cracks localised around mid-span. The ultimate load decreased to 163.04 kN in the numerical analysis, aligning with experimental reductions due to diminished shear capacity. **Figure 6** shows the effect of the shear span to depth ratio on the crack pattern. In the experimental program, similar behaviour was observed. Beams with higher *a/d* ratios demonstrated more flexible responses and wider mid-span cracks, while those with smaller ratios showed increased shear contribution and improved load transfer efficiency. The transition from shear-arch to flexural mechanism with increasing *a/d* was captured in both the damage pattern and deflection profiles of the FE models. These consistent trends validate the robustness of the theoretical approach in simulating key geometric parameters and provide insight into optimal design choices for slender beam elements.

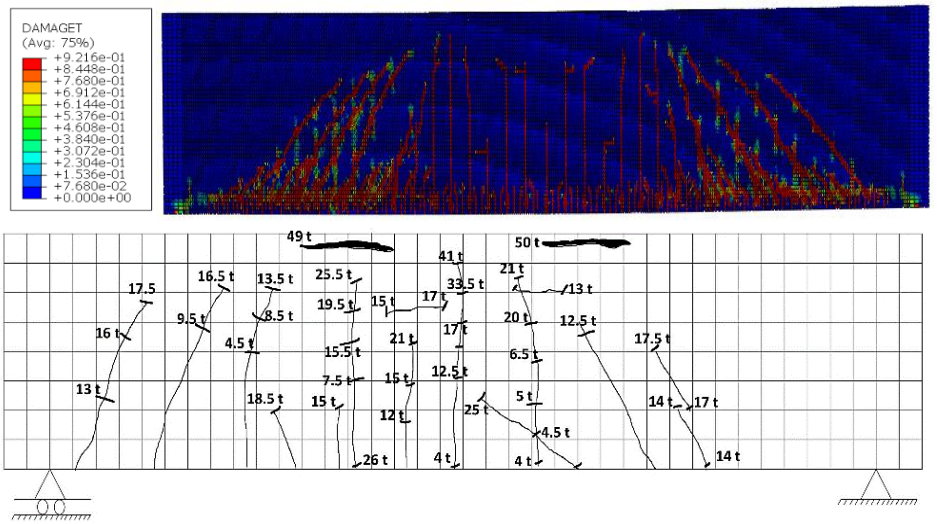

(a)

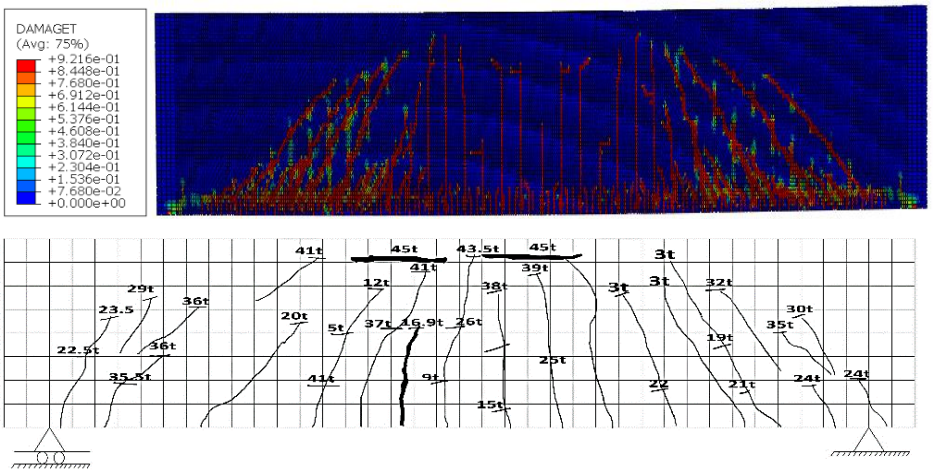

(b)

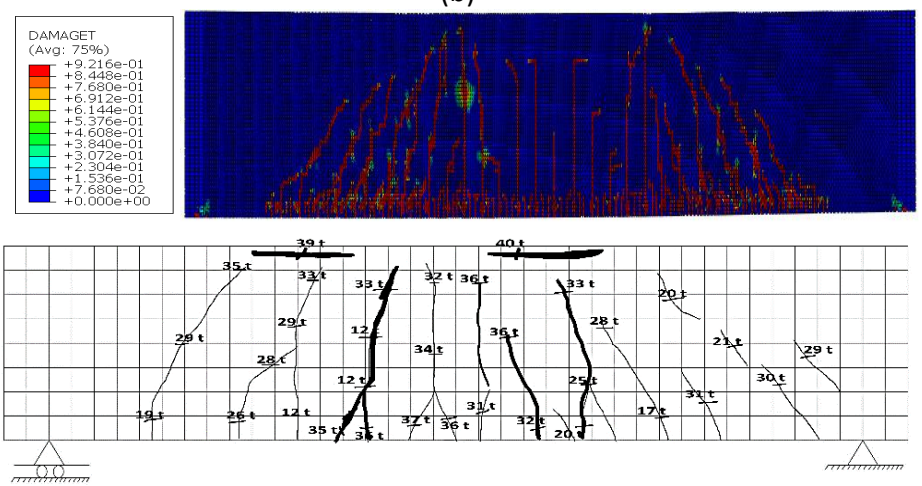

(c)

Figure 5: Effect of Reinforcement ratio on the crack patterns.
(a) Specimen **B3,** (b) Specimen **B4,** (c) Specimen **B7.**

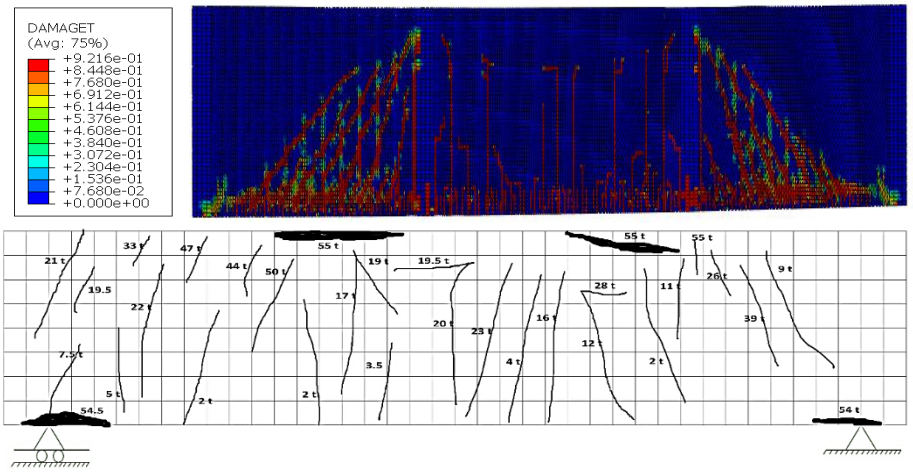

(a)

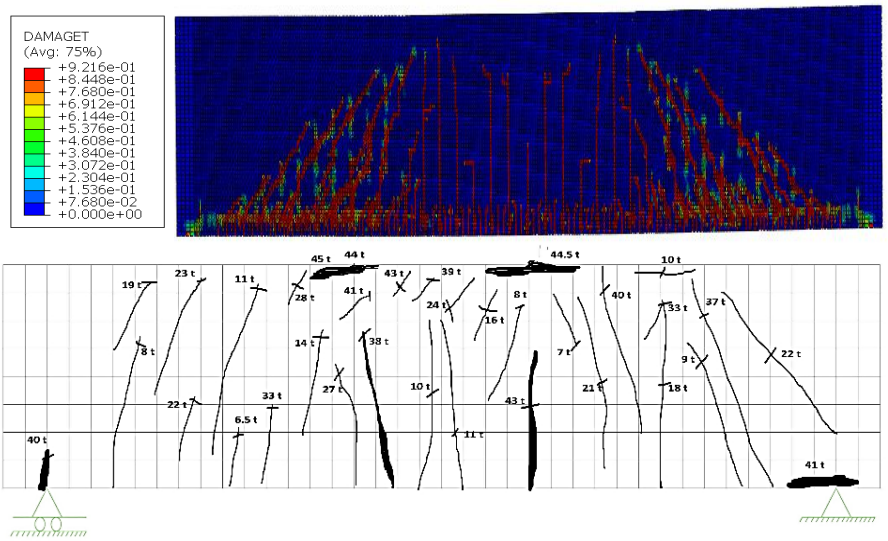

(b)

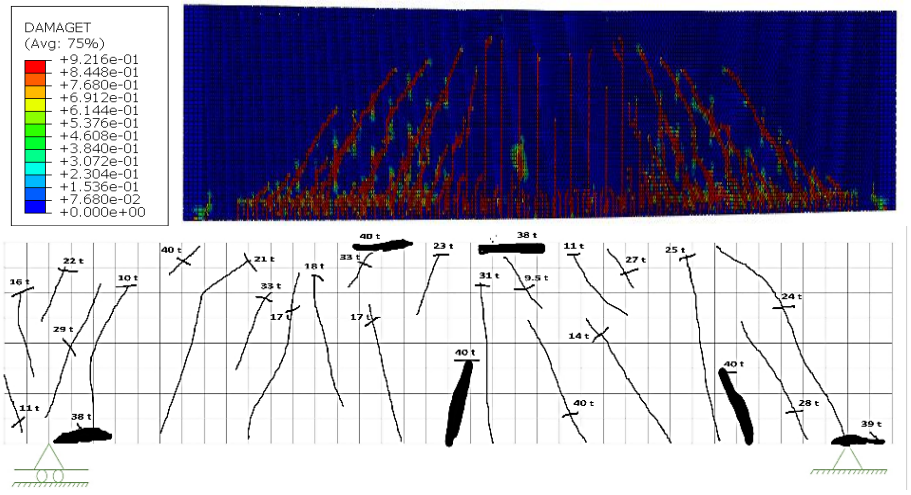

(c)

Figure 6: Effect of the shear span-to-depth ratio on the crack patterns. (a) Specimen **B8,** (b) Specimen **B9,** (c) Specimen **B10.**

- **Effect of Reinforcement ratio on the deflection**

Figures 6 to 8 show the deflection of the beam model obtained from FE results. The maximum deflection values obtained at the ultimate load were 14.68 mm, 10.66 mm, 11.22 mm, 10.88 mm, 11.88 mm, 0.0014 mm, 10.34 mm, 10.02 mm, 10.39 mm and 10.16 mm for specimens **B1**, **B2**, **B3**, **B4**, **B5**, **B6**, **B7**, **B8**, **B9** and **B10**, respectively.

Beam 1 appears to have the largest deflection (14.68 mm), which is shown in deep blue in the bottom centre of the image. The colour gradient in the image likely represents the magnitude of the deflection, with red indicating the largest deflection and blue indicating the smallest deflection. It is clear to us from this figure that most of the beams deflected and that they did not resist deflection well. **Figure 7** shows the deflection behaviour for beam **B1**.

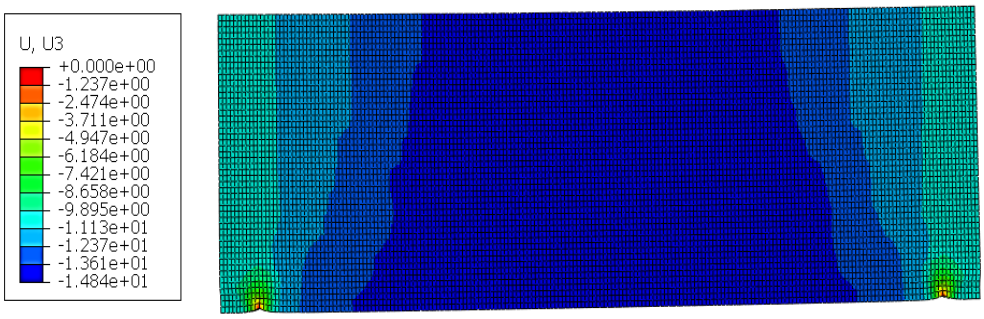

Figure 7: The deflection behaviour for beam (**B1**).

For beam **B2**, according to **Fig. 8 (a)**, it was noted that the highest concentration of stresses occurs in the bottom portion of the beam, near the supports and the beam has undergone some deformation under the applied load, with areas in green and red exhibiting greater deformation. Also, we can notice similarities in deformations and cracks on both sides of the concrete beam. As usual, small cracks appear at the beginning of loading in the centre of the beam and increase to become larger cracks in width, and the first actual visible crack begins when the loading becomes 8 tons. As the load increases, the cracks begin to spread and move to the edges of the beam, forming inclined flexural cracks, so that the crack starts from the supports to the load area. The beam collapsed at a load of 45 tons and the type of failure was flexural failure. The distribution of stresses and deformations in the beam caused by loading is depicted at **B5** in **Fig. 8 (b)** No cracks appeared at the beginning of the load, and it held up until the load reached 9 tons when the first crack appeared. As the load increases, the number of cracks begins to increase as well. As the load grows, microcracks gradually become deep cracks until the failure occurs at 50 tons. Shear failure was the cause of this beam's failure.

The crack pattern of the theoretical FE model of the **B6** specimen is shown in **Fig. 8 (c)**. This beam is similar to **B5** in terms of the pattern of cracks, starting from the appearance of very small cracks, through the first crack, until the failure crack. The micro-cracks started late in the back, at a load of 8 tons, and then the first crack appeared at a load of 10 tons at the bottom of the middle of the beam. These cracks were small vertical and when the load began to increase, the cracks began to appear densely at the edges the supports at the bottom and the load places at the top. When the load reached its maximum at 55 tons, we found that the beam had completely flexurally failed.

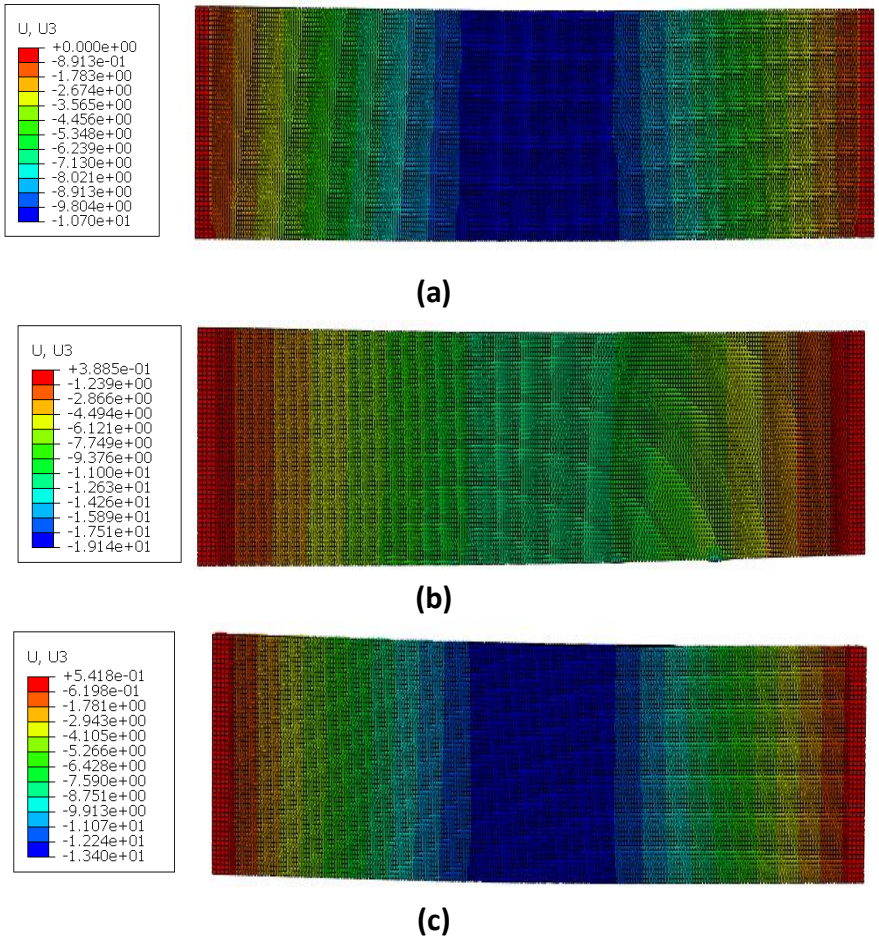

Figure 8: Effect of Concrete Strength on the deflection:
(a) Specimen **B2,** (b) Specimen **B5,** (c) Specimen **B6.**

Figure 9 (a) shows us the crack pattern of the theoretical FE model of the beam B3 specimen. With the start of operation of the testing machine, and as soon as the load reached 1t, micro-cracks began to appear in the middle of the bottom of the beam, and suddenly, the first crack appeared at a load of 4 tons. As the load gradually increased, the cracks increased in the middle, and then new, larger cracks began to form at the load points and the supports. We began to notice the beginning of the collapse of the beam when the load reached 48 tons, but it held out until it reached a state of total collapse when the load reached 50 tons. Also, the type of failure was a flexural failure.

For the beam B4, the crack pattern of the theoretical FE model is displayed in Fig. 9 (b). Microcracks started to form in the center of the beam's bottom as soon as the testing machine started operating. Suddenly, the first crack from a load of 3 tons appeared.

The central cracks grew larger as the load progressively increased, and new, larger cracks started to emerge at the supports and the load points. When the load hit 44 tons, we could see the beam was starting to collapse, but it held out until the load reached 45 tons, at which point it completely failed. Furthermore, it was a flexural failure.

The failure patterns of B7 differ greatly from those of its counterparts. Microcracks began to appear when loading 11 tons, and these cracks appeared densely at the bottom of the beam, specifically between the supports. The microcracks continued to spread until the load reached 12 tons, where the first crack in the beam that was detected began to appear. What is also different in

the failure behaviour of this beam is that all the cracks spread in the middle part of the beam. We were also surprised that the failure began in the middle of the beam early, when the load was 38 tons, and it failed when the load was 41 tons. The type of failure of the beam was also flexural failure as shown in Fig. 9 (c).

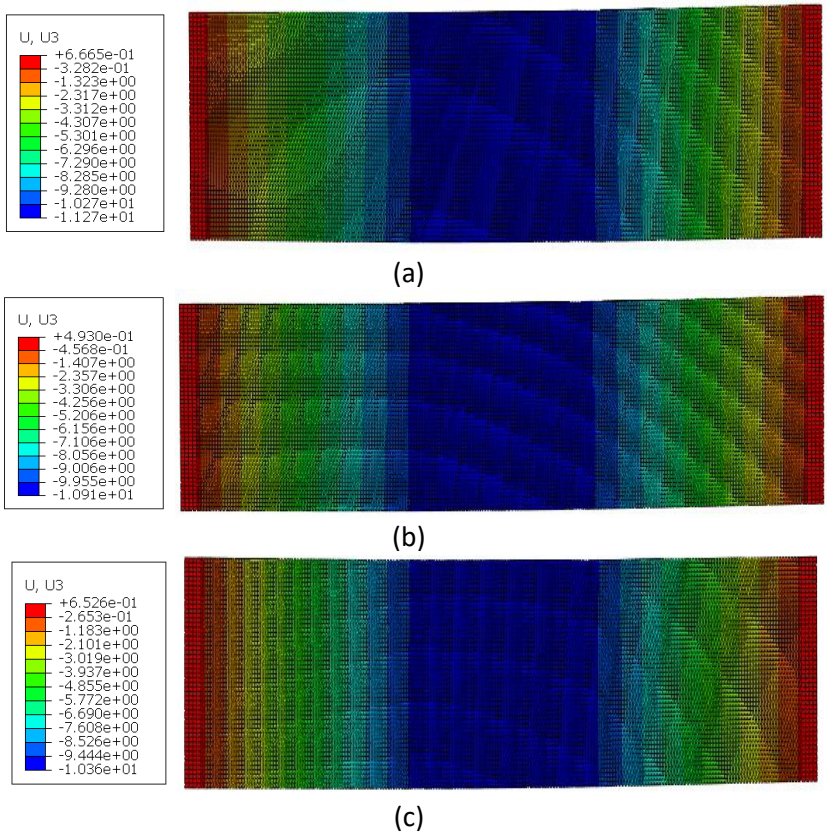

Figure 9: Effect of Reinforcement ratio on the deflection.
(a) Specimen **B3,** (b) Specimen **B4,** (c) Specimen **B7.**

For the beam B8, the crack pattern of the theoretical FE model is displayed in Fig. 10 (a). Immediately after the testing apparatus was turned on, microcracks appeared in the middle of the bottom of the beam. Early and suddenly, the first crack from a load of 2 tons appeared. We observed that existing cracks grew larger as the load increased. This indicates progressive damage in the concrete, where initial cracks weaken the structure and allow further cracking under higher loads. The formation of new, larger cracks at stress points and supports suggests that these areas became overloaded as the existing cracks compromised the beam's capacity. The beam showed signs of potential collapse at 35 tons, indicating significant structural weakness. This could involve increased deflection, widening cracks, or localised crushing of concrete. The complete collapse at 45 tons marks the final point of failure. The beam could no longer sustain the load and likely experienced a sudden and complete structural breakdown. It identified the failure mode as a flexural failure.

Fig. 10 (b), the distribution of loading-induced stresses and deformations in the beam at B9. The load was stable initially, showing no cracks until it reached 6.5 tons, at which point the first crack showed up. The number of cracks starts to rise in tandem with the load. Microcracks progressively deepen into cracks as the load increases, failing at 45 tons. The reason for this beam's failure was shearing failure.

The crack pattern of the theoretical FE model of the beam B10 is shown in Fig. 10 (c). Immediately after the testing apparatus was turned on, microcracks began to appear in the middle of the bottom of the beam. As the load increases more and more, micro cracks begin to gradually turn into deep cracks and the first crack of the beam in the FE model corresponds to a load of 9.5 tons. The beam began to failure when the load reached 40 tons. The failure mode for this beam was a shear failure. The dense concentration of microcracks at the bottom of the beam, specifically between the supports, indicates a potential flaw or stress concentration point in that area. This could be due to imperfections in the concrete, or geometrical factors or else.

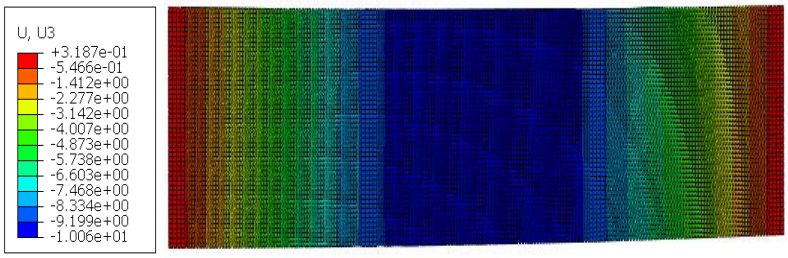

(a)

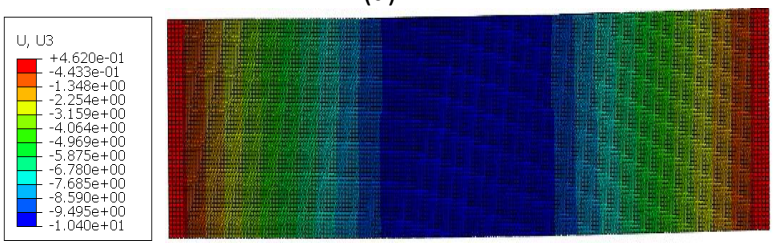

(b)

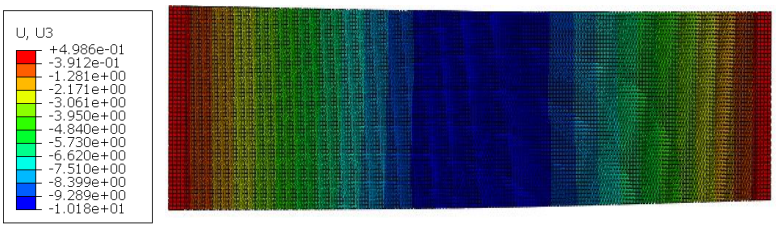

(c)

Figure 10: Effect of the shear span-to-depth ratio on the deflection.
(a) Specimen **B8,** (b) Specimen **B9,** (c) Specimen **B10.**

3.2. The comparison between experimental and theoretical results

The comparison of first crack load, ultimate load, and mid-span deflection between experimental and FE simulation results is shown in **Table 5.** The Table indicates that when compared to experimental results, FE simulations obtain accurate and compatible results. It is discovered that the average first crack load difference as a percentage is around 6.86 %. However, the average ultimate load difference as a percentage is around 3.48 % and 8.82 % for the average maximum mid-point deflection. **Fig. 11** shows the relationships between the applied load and both experimental first crack loads, F.E. first crack loads, experimental ultimate loads, F.E. ultimate loads, experimental maximum deflection, and F.E. maximum deflection of all tested beams.

From the following results, it appears that the experimental first crack load values (**EXP**) are generally lower than the theoretical first crack load values (**FEM**) for most beams. This suggests that the theoretical model predicts a slightly higher first crack load than what is observed in the experiment.

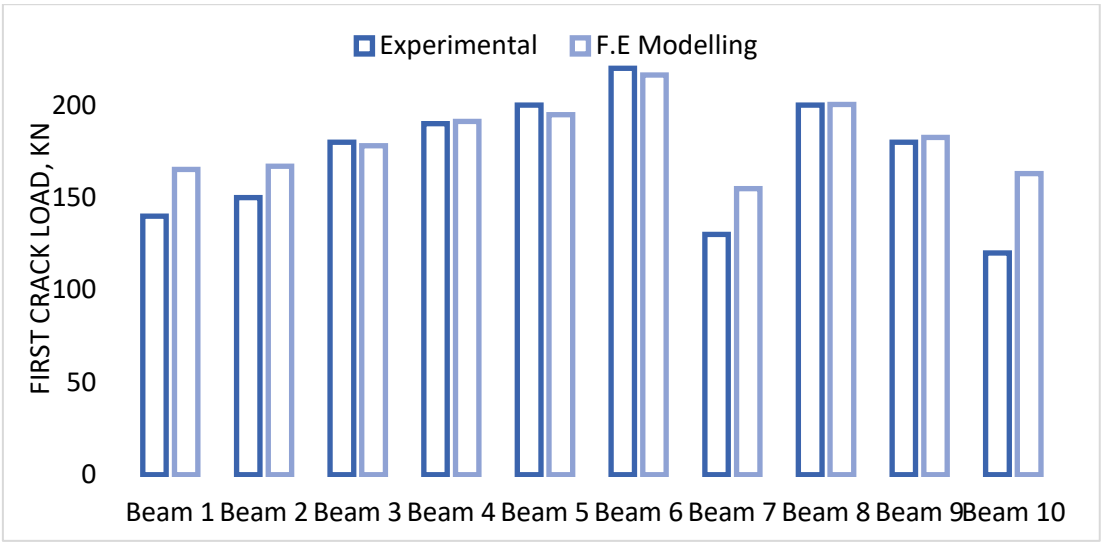

(a)

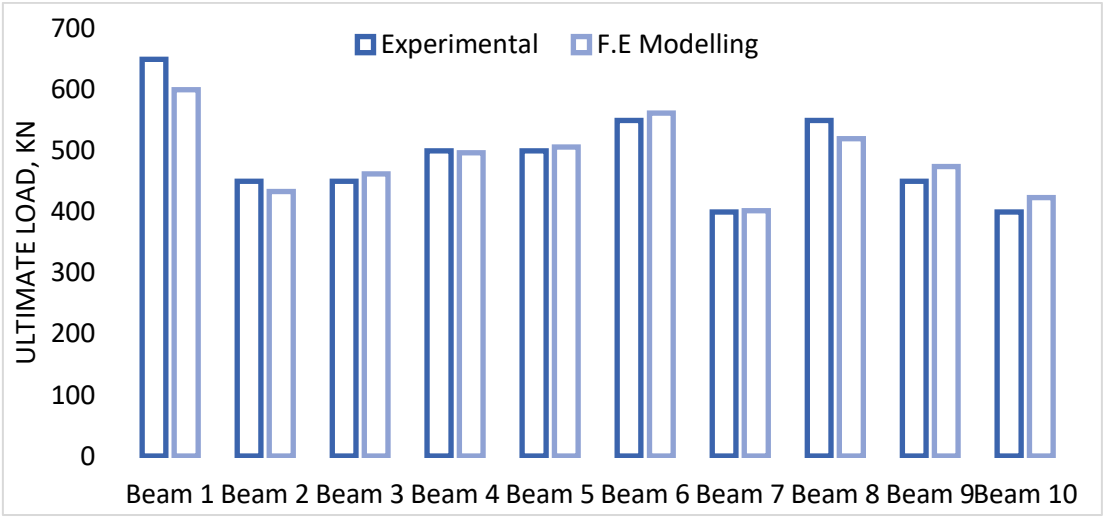

(b)

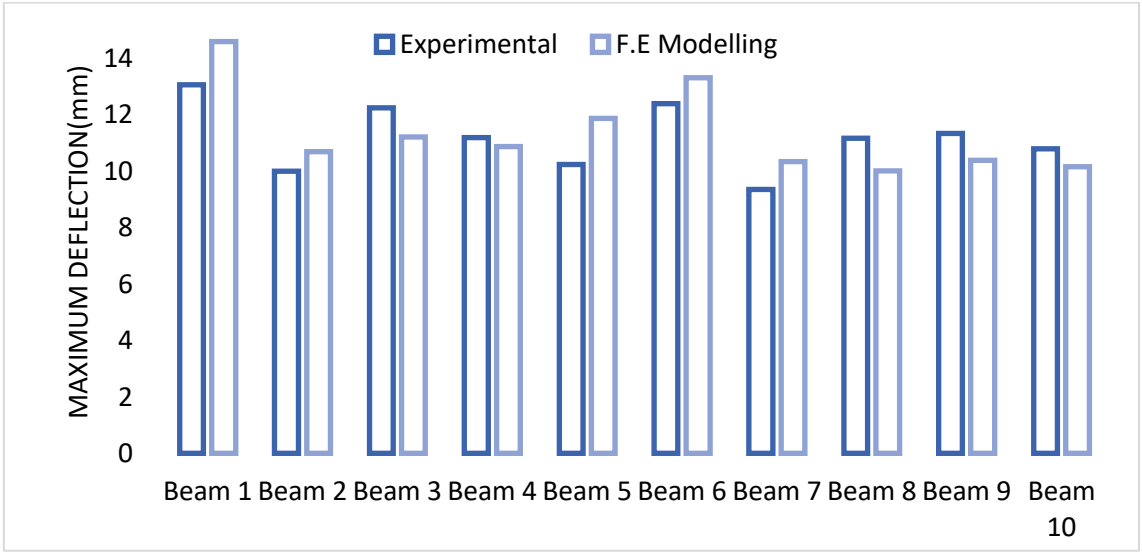

(c)

Figure 11: The comparison between the experimental and F.E. results for all tested beams. (a) The first crack load, (b) The ultimate load, (c) The maximum deflection.

Table 5: Comparison between Experimental and Finite Element (F.E.) Results.

Beam Specimen	First Crack Load (P_{cr}), kN			Deflection at Ultimate Load (Δ_u), mm			Ultimate Load (P_u), kN		
	Exp	FEM	Diff %	Exp	FEM	Diff %	Exp	FEM	Diff %
Beam 1	11.7	14.6	13.07	7.6	600.18	650	17.9	165.17	140
Beam 2	7	10.7	10	3.6	433.54	450	11.2	166.93	150
Beam 3	8.4	11.22	12.25	2.7	462.41	450	10.6	178.08	180
Beam 4	2.8	10.88	11.2	0.6	496.61	500	0.6	191.29	190
Beam 5	16	11.88	10.24	1.2	506.14	500	2.5	194.9	200
Beam 6	7.4	13.32	12.4	2.1	561.79	550	1.6	216.31	220
Beam 7	10.4	10.34	9.36	0.5	402.13	400	19.1	154.87	130
Beam 8	10.2	10.02	11.17	5.4	520.17	550	0.1	200.37	200
Beam 9	8.4	10.39	11.34	5.3	474.06	450	1.4	182.58	180
Beam 10	5.9	10.16	10.8	5.8	423.29	400	3.6	163.04	120
Average			**6.86%**			**3.48%**			**8.82%**

3.3. The Comparison of Load-Deflection Curves

One of the most significant results that has been used to predict specimen rigidity and strength is the deflection of the specimen's midpoint. The middle of the specimen was chosen, especially since it is where the maximum deflection occurred. **Figures. 12 to 14**, show the values of measured loads and deflections acquired from the experimental tests, in comparison with the corresponding values acquired from the FE modelling for the same tested beams. According to the numerical analysis, the behaviour of the load-deflection curves accurately anticipated the actual behaviour of the tested beams and was consistent with the experimental results for all models.

Figure 12 illustrates the load-deflection curves for beams **B2 (a)**, **B5 (b)**, and **B6 (c)**, all of which are made from high-strength self-compacting concrete and differ in concrete compressive strength. In all three cases, the initial portions of the curves - at lower load and deflection levels-show good agreement between the experimental results and the finite element model (FEM) predictions. This indicates that the FEM simulations effectively capture the initial elastic behaviour and stiffness of the beams. As the load increases and the beams transition into the nonlinear range (evidenced by a decreasing slope in the curves), the FEM results generally follow the trend observed in the experimental data. This suggests that the models are capable of simulating both cracking and material nonlinearity in high-strength self-compacting concrete.

Both the experimental and FEM curves show a clear degradation in stiffness with increasing load, indicating that the beams become progressively less stiff due to cracking and material yielding. The FEM models appear to capture this stiffness degradation with reasonable accuracy. This comparison indicated that the different ratios between the numerical and the experimental maximum deflection were 11.2%, 2.5% and 1.6%, for beams **B2**, **B5**, and **B6,** respectively.

The figures presented illustrate the load-deflection curves for beams **B3(a)**, **B4(b)**, and **B7(c)**. These beams are made from high-strength self-compacting concrete and exhibit different reinforcement ratios as shown in **Fig. 13.**

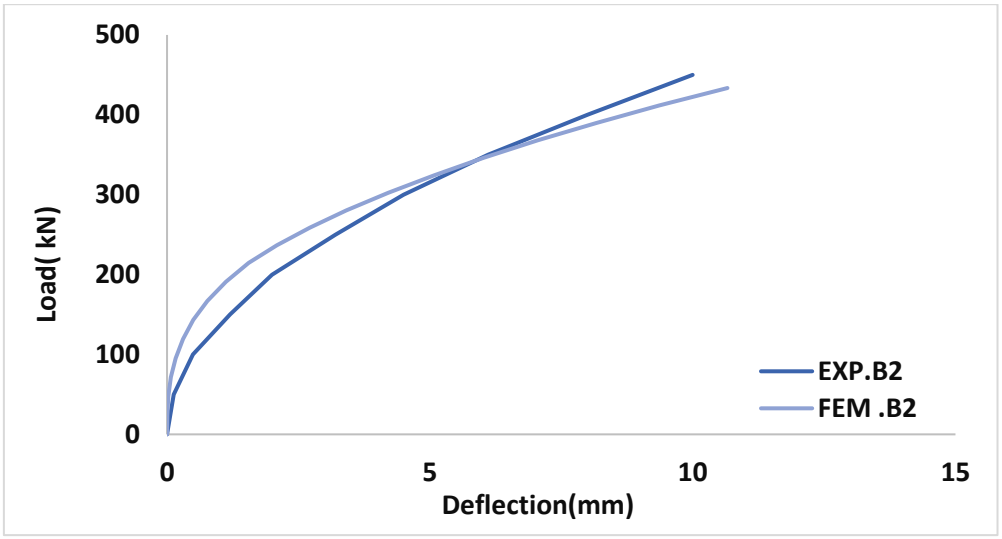

(a)

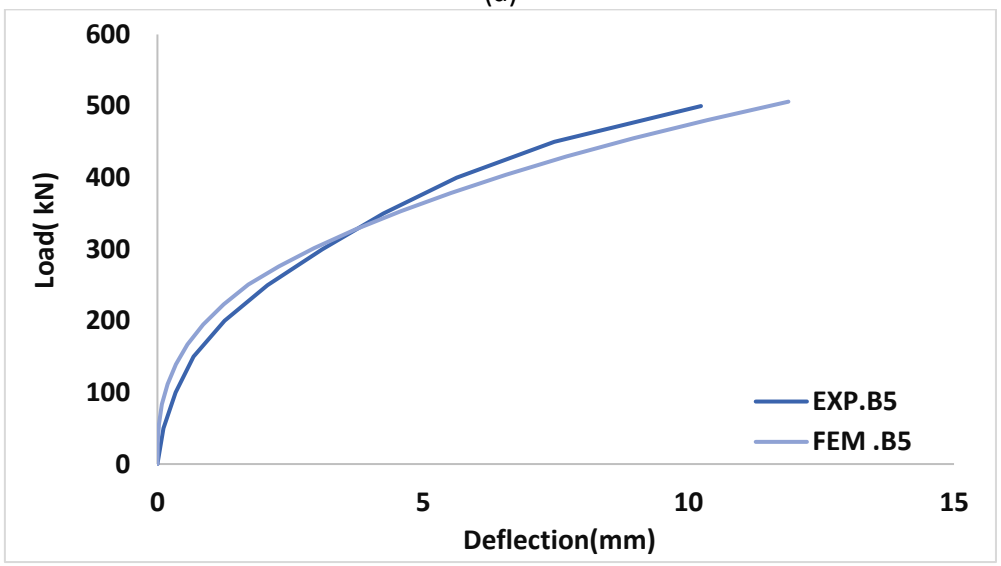

(b)

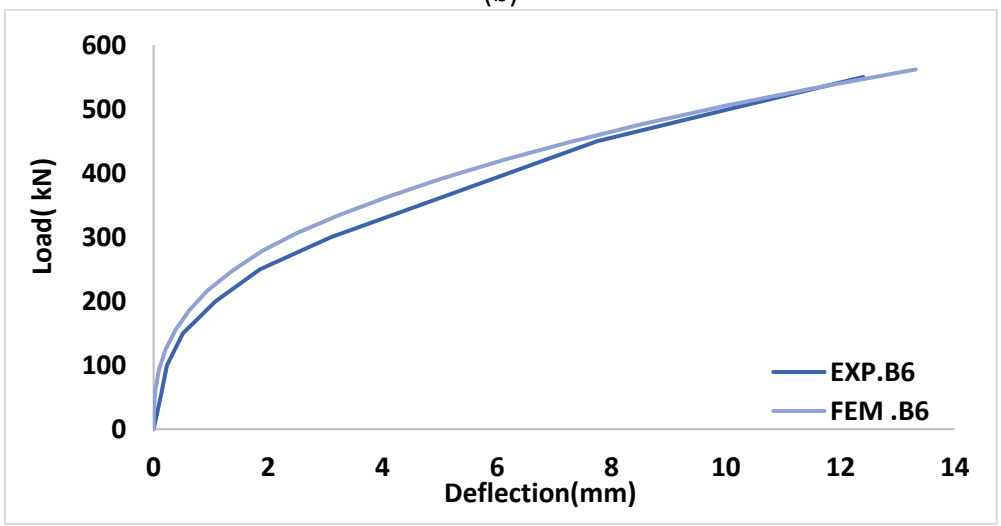

(c)

Figure 12: Experimental and F.E. load-deflection curves of specimens that varied in concrete strength. (a) Specimen **B2**, (b) Specimen **B5**, (c) Specimen **B6**.

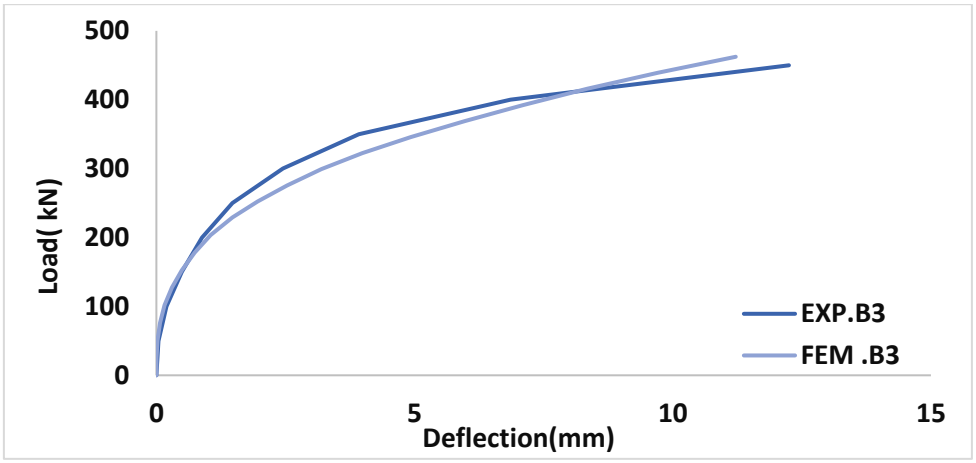

(a)

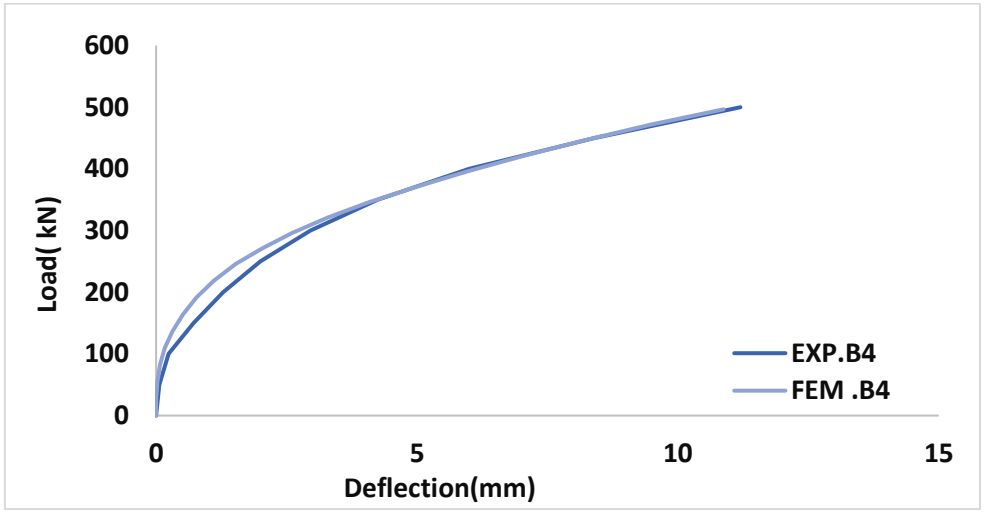

(b)

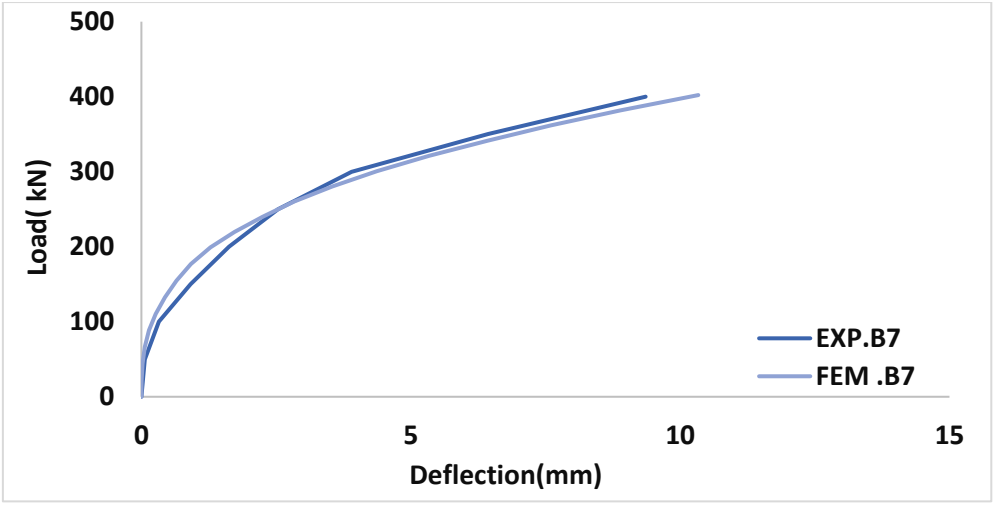

(c)

Figure 13: Experimental and F.E. load-deflection curves of specimens that varied in reinforcement ratio.

(a) Specimen **B3**, (b) Specimen **B4**, (c) Specimen **B7**.

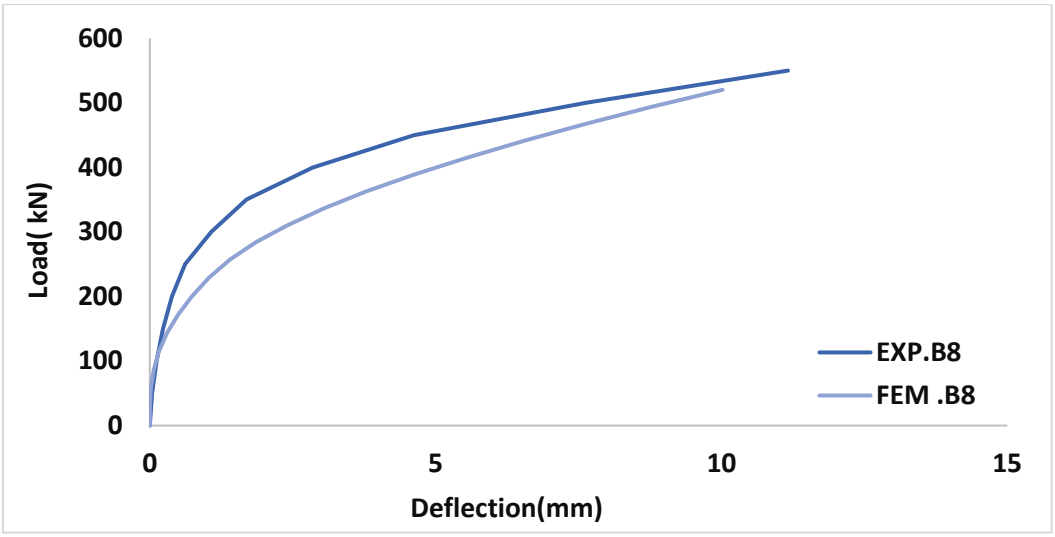

(a)

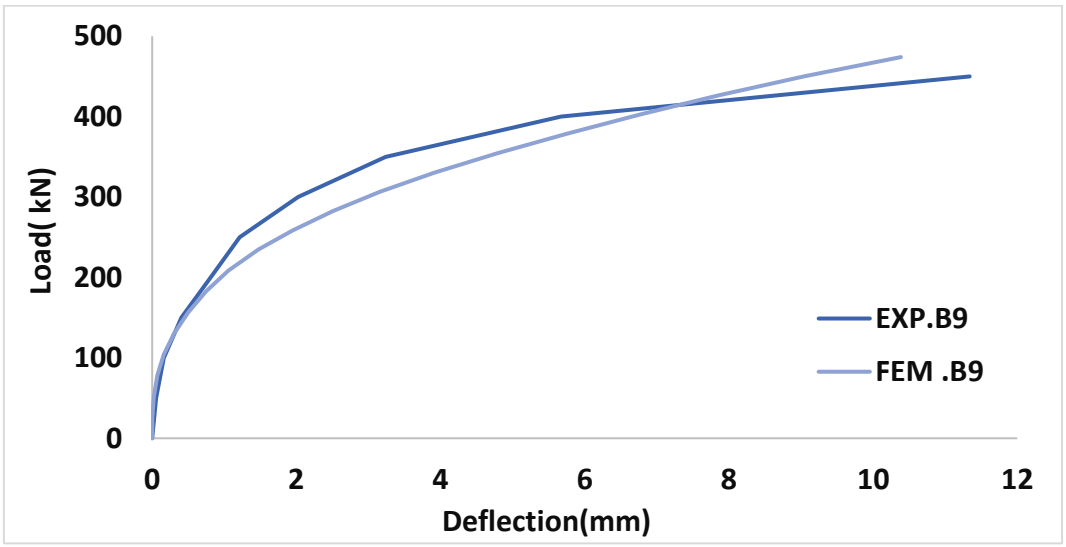

(b)

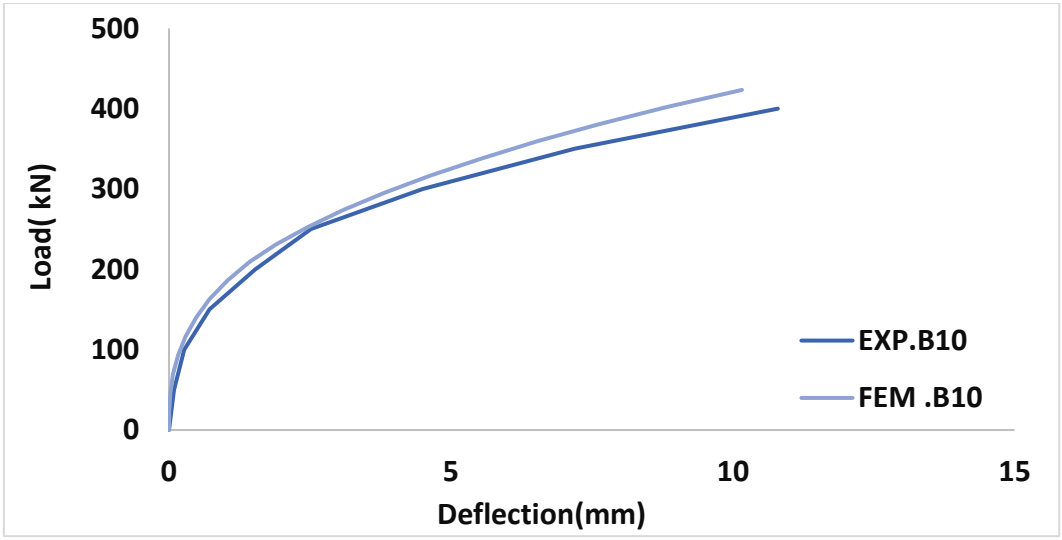

(c)

Figure 14: Experimental and F.E. load-deflection curves of specimens that varied in shear span to depth ratio. (a) Specimen **B8**, (b) Specimen **B9**, (c) Specimen **B10**.

At the beginning, when the loads and deflections are low, the experimental results and FEM results for all three beams match well, showing that the FEM models accurately reflect the initial stiffness of the high-strength self-compacting concrete beams, no matter how much reinforcement is used. As the load increases and the beams begin to crack and yield, both the experimental and FEM results exhibit a similar pattern of decreasing stiffness. This indicates that the FEM models effectively capture the initial stiffness of the high-strength self-compacting concrete beams regardless of the reinforcement ratio.

As the load increases and the beams enter the non-linear range (due to concrete cracking and steel yielding), both experimental and FEM curves exhibit a similar trend of stiffness degradation. The FEM models generally follow the experimental trend, demonstrating their capability to simulate the complex, non-linear behaviour influenced by varying reinforcement.

It's expected that a higher reinforcement ratio would generally lead to higher ultimate load capacity and potentially higher stiffness. The curves should reflect these trends. From these curves, we can conclude that the differences in the numerical and experimental maximum deflections were 10.6%, 0.6%, and 19.1%, for beams **B3**, **B4**, and **B7,** respectively. **Figure 14** depicts the load-deflection behaviour of beams **B8(a)**, **B9(b)**, and **B10(c)**, which differ in their shear span-to-effective depth ratios (*a/d* ratios). As the applied load increases and the beams transition into the nonlinear phase, primarily due to cracking and subsequent material yielding, both the experimental and finite element method (FEM) curves show a noticeable reduction in stiffness. The FEM simulations closely replicate the experimental trends, indicating their effectiveness in modelling the complex nonlinear response, which is significantly influenced by the *a/d* ratio. The *a/d* ratio plays a crucial role in determining the beam's failure mechanism and its overall structural behaviour under loading. Lower *a/d* ratios typically correspond to shear-dominated behaviour, whereas higher *a/d* ratios are associated with flexure-dominated responses. This distinction has a direct impact on the shape and characteristics of the load-deflection curves observed in both experimental and numerical analyses. Finally, the different ratios between the experimental and the numerical maximum deflection were 0.1%, 1.4% and 3.6% for beams **B8**, **B9**, and **B10,** respectively.

4. CONCLUSIONS AND RECOMMENDATIONS

This study presented an integrated experimental and numerical investigation into the structural behaviour of high-strength self-compacted reinforced concrete (HS-SCRC) slender beams subjected to static four-point flexural loading. The experimental phase provided reliable data on crack patterns, deflection behaviour, failure modes, and strain development for ten beam specimens with varying concrete strengths, reinforcement ratios, and shear span-to-depth (*a/d*) ratios. Subsequently, a finite element model was developed in ABAQUS using the Concrete Damaged Plasticity (CDP) model for concrete and an elastic–plastic model for reinforcing steel. The simulation results showed strong agreement with the experimental findings, validating the numerical modelling approach.

The numerical models were able to accurately replicate key structural behaviours such as initial cracking, ultimate load capacity, post-cracking deflection, and strain localisation. The observed failure mechanisms - whether flexure-dominant or shear-flexure interaction - were consistently predicted by the simulations. The average discrepancies between the experimental and numerical

results were within acceptable engineering tolerances, with only 6.86% for the first cracking load, 3.48% for the ultimate load, and 8.82% for the mid-span deflection.

More importantly, the parametric investigation revealed the critical role of each design factor. Higher concrete strength significantly improved the beams' stiffness and ultimate strength, while increasing the reinforcement ratio enhanced ductility, reduced deflection, and delayed steel yielding. A reduction in the *a/d* ratio activated beneficial arching behaviour and increased shear resistance. These findings confirm that the structural performance of HS-SCRC slender beams is highly sensitive to these parameters, and careful consideration is essential during the design process.

Overall, the validated finite element model provides a powerful analytical tool for predicting the nonlinear performance of HS-SCRC slender beams. It enables detailed insight into internal damage evolution and strain development and can be used to optimize structural designs and support future updates to design guidelines and codes. This research contributes to advancing both the theoretical understanding and practical application of high-performance slender concrete elements in modern structural engineering.

From the results obtained through this work, the following subjects can be recommended for studying in future:

- Extensive experimental and theoretical studies are required to determine and understand the behaviour of high-strength slender concrete under repeated and cyclic loading.
- Many variables must be studied, not only the reinforcement steel, compressive strength and span-to-depth ratio, but it is also possible to study the distance between the stirrup bars as a variable.
- Behaviour of rectangular high-strength concrete slender reinforced beams with hybrid reinforcement (steel and FRB).
- Further work is needed to investigate the effect of ductility in this type of concrete beam.
- Further research is needed to study the structural behaviour of concrete slender beams reinforced with FRP bars instead of steel reinforcing bars.

REFERENCES

[1] Jum'ah, O., Mahmood, M. A., & Abdullah, A. Shear behaviour of reinforced concrete beams made with different strength grades of fiber-reinforced self-compacting concrete. Structures, 2021, 33, 4223–4235.

[2] Hussein, T. H. A., & Khudhair, J. A. S. Experimental and numerical evaluation of shear strength of directly and indirectly loaded flanged recycled self-compacted reinforced concrete deep beams. Journal of Engineering, 2020, 2020(1).

[3] Kalkan, I & Kartal, S. Torsional rigidities of reinforced concrete beams subjected to elastic lateral torsional buckling. International Journal of Civil and Environmental Engineering, 2017, 11(7), 905–910.

[4] Kalkan, I. Lateral torsional buckling of rectangular reinforced concrete beams. ACI Structural Journal, 2014, 111(1), 123–132.

[5] Tahenni, T., Bouziadi, F., Boulekbache, B., & Amziane, S. Experimental and nonlinear finite element analysis of shear behaviour of reinforced concrete beams. Structures, 2021, 29, 1582–1596.

[6] ANSYS – Engineering Analysis System. Theoretical Manual (for ANSYS Revision 8.04), Swanson Analysis

Systems (1998).

[7] ABAQUS Documentation User's Guide: ABAQUS User's Guide: Dassault Systèmes, Simulia Corp, Providence, 2021.

[8] Elwakkad, Noha Yehia, Bassam A. Tayeh, Ghada Mousa Hekal, and Khaled Mohamed Heiza. "Experimental and Numerical Investigation of the Behaviour of Self-Curing RC Flat Slabs." Case Studies in Construction Materials 17, 2022, e01457.

[9] ABAQUS Documentation User's Guide: ABAQUS User's Guide: Dassault Systemes, Simulia Corp, Providence, 2018.

[10] Megarsa, Edosa, and Goshu Kenea. "Numerical Investigation on Shear Performance of Reinforced Concrete Beam by Using Ferrocement Composite." Mathematical Problems in Engineering 2022 (2022).

[11] Attia, Mohammed M., Bassam Abdelsalam Abdelsalam, Dina E. Tobbala, and Basem O. Rageh. "Flexural Behaviour of Strengthened Concrete Beams with Multiple Retrofitting Systems." Case Studies in Construction Materials, 2023, 18, e01862.

[12] Dinsenbacher, A. L., and F. E. Brauer. "Material Development, Design, Construction, and Evaluation of a Ferro-Cement Planing Boat." Marine Technology and SNAME News, 1974, 11, 03: 277-295.

[13] Shaheen, Y. B., Mohamed A. Safan, and M. Abdalla. "Structural behaviour of composite reinforced ferrocement plates." Concrete Research Letters, 2012, 3, 3: 477-490.

[14] E.C.P. 203/2020, Egyptian Code of Practice: Design and Construction for Reinforced Concrete Structures. Cairo, Egypt, 2020.

[15] Rageh, B. O., El-Mandouh, M. A., Elmasry, A. H., & Attia, M. M. Flexural behaviour of RC beams strengthened with GFRP laminate and retrofitting with novelty of adhesive material. Buildings, 2022, 12(9), 1444.